8

Tungsten Oxide Nanorods: Synthesis, Characterization, and Application

Erik H. Williamson and Nan Yao

8.1. INTRODUCTION

In recent years, transition metal oxide structures have garnered considerable attention due to their unique properties. Among the numerous transition metal oxides, tungsten oxides have been of special interest because of their distinctive characteristics that have led to a number of applications and promise further developments. Such applications include gas and humidity sensors, optical devices, electrochromatic windows, catalysts, and many more.[1–6] These properties even include high temperature superconductivity—sodium-doped tungsten oxide is thought to be a high temperature superconductor with a $T_c \approx 90$ K.[7] Numerous forms of tungsten oxide have been synthesized, with the stoichiometric formulas for all of forms being WO_x, where $0 < x \leq 3$. Bulk tungsten oxides as well as tungsten oxide films are generally WO_3, with WO_2 forms also possible under some conditions. With the great interest in nanoscience and nanostructured materials over the past 15 years, researchers have developed nanostructured forms of tungsten oxide as well. These have ranged from WO_3 nanocrystals on the order of only a few nanometers to one-dimensional nanorods of nonstoichiometric composition ranging from $WO_{2.5}$ to $WO_{2.9}$ (referred to as nanowires, nanoneedles, or nanowhiskers by some researchers).

Princeton University, Princeton Institute for the Science and Technology of Materials, 70 Prospect Avenue, Princeton, NJ 08540

The nanorod form of tungsten oxide presents both exciting possibilities and some special challenges.[8,9] In particular, tungsten oxide nanorods can be used as a template for the synthesis of WS_2 nanotubes via direct reaction with H_2 and H_2S.[10] These nanotubes have important applications as solid lubricants and as tips for atomic force microscopy.[11] Besides use as a template, the unusual defect structure of $WO_{2.72}$ ($W_{18}O_{49}$) nanorods could be exploited for various applications such as gas sensing and catalysis.[12] Synthesis of these structures, however, has been challenging. Until recently, most methods have involved high temperature vapor or vapor–solid processes.[12,13] Using these processes, it was difficult to achieve a controlled, relatively monodisperse nanorod size. Over the past few years, a number of groups have developed innovative methods to overcome these limitations. Simultaneously, the body of literature on the applications of tungsten oxides has grown, allowing unique insights into the physical processes that govern these applications. This study will review some of these synthetic methods and discuss what these and other studies have elucidated about the structure and properties of tungsten oxide nanorods. The applications of such nanorods will then be addressed, again in light of the literature.

8.2. TUNGSTEN–OXYGEN CHEMISTRY

8.2.1. Oxidation and Reduction of Tungsten and Tungsten Oxides

The chemistry of tungsten and its oxides is well understood for a few compounds, but due to the richness and complexity of the tungsten–oxygen system, this knowledge is far from comprehensive. The complexity of the tungsten–oxygen system is shown in tree representation of the various classes of oxides in Fig. 8.1. In most of these oxides, tungsten is predominately in the W^{+6} oxidation state, with 6 oxygen atoms

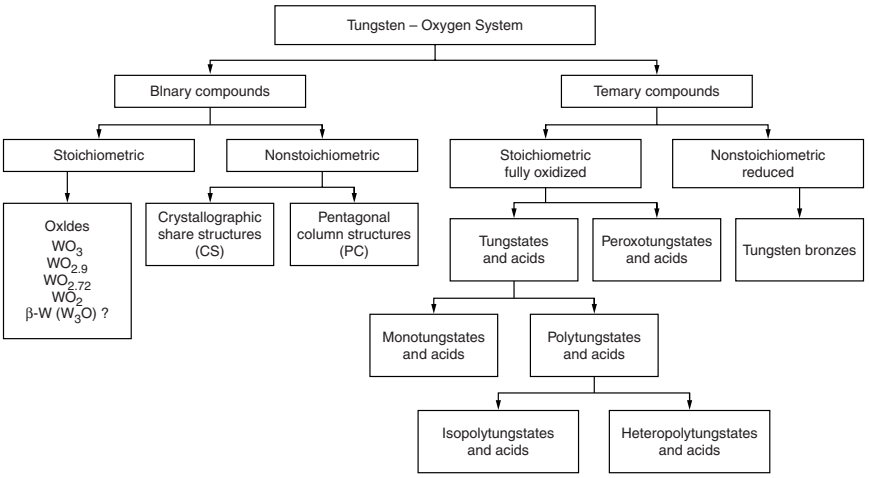

FIGURE 8.1. A summary of the tungsten–oxygen system. From Lassner and Schubert.

surrounding each tungsten atom in an octahedral configuration. In fully oxidized tungsten (WO_3), these octahedra are arranged in a corner-sharing configuration. In reduced oxides (WO_x, $2 < x < 3$), intricate combinations of corner-, edge-, and face-sharing arrangements WO_6 octahedra are frequently present. Further complicating the crystallographic structure of these compounds are the WO_4 tetrahedra and WO_7 pentagonal bipyramids that are frequently found in fully oxidized and partially reduced oxides respectively. With such a vast array of configurations, it is no wonder that several hundreds or thousands of tungsten oxides have been discovered.[14]

Tungsten metal can be easily oxidized in air or oxygen to form oxides. When occurring at temperature up to 327°C, this reaction forms WO_3, with the thickness of the oxide layer dependent on both temperature and humidity. From 327°C to 400°C, a protective oxide layer of oxide is formed, though there is currently some question as to its composition (it has been reported as $WO_{2.75}$, but this figure has been disputed). Above 600°C, a WO_3 layer is produced as the initial protective oxide becomes fully oxidized. WO_3 is quite permeable to oxygen, so the $WO_{2.75}$ layer continues to be oxidized to the trioxide form, with the rate being governed by the diffusion of tungsten ions to the $WO_{2.75}$–WO_3 boundary. Sublimation of WO_3 begins at 750°C, becomes substantial at 900°C, and reaches the rate of oxidation above 1300°C, thus leaving the tungsten surface bare of oxide above this temperature. The log of the rate of oxidation from 700 to 1300°C has been shown to be proportional to $P_{O_2}^{1/2}/T$, where P_{0_2} is the partial pressure of oxygen and T is the absolute temperature.[15]

Oxidation of tungsten with water and reduction of tungsten oxides with hydrogen are quite similar, with the high partial pressure of water or hydrogen driving the reaction in a particular direction. The oxidation reaction has been found to follow this sequence of reactions:

$$\begin{aligned} W + 2H_2O &\rightarrow WO_2 + 2H_2 \\ W + 3H_2O &\rightarrow WO_3 + 3H_2 \\ WO_3 + xH_2O &\rightarrow WO_3 \cdot xH_2O \end{aligned}$$

This reaction with water at 38°C is very slow and increases with increasing temperatures and pressures. Reaction with water vapor between 20 and 500°C leads strictly to the formation of WO_3—no other oxides are formed. The rate of this reaction has been found to be dependent on temperature and the ratio of the partial pressure of water to that of hydrogen. However, by adjusting these partial pressures properly, all known oxides can be formed. When both are low, WO_2 is formed. As these pressures increase, the more oxidized forms are produced ($WO_{2.72}$, $WO_{2.9}$, and finally WO_3). Additionally, higher temperatures favor the more oxidized forms. It also must be noted that hydrated oxides can be easily volatilized above about 900°C, with most volatile form being $WO_2(OH)_2$.[15] Such volatile compounds may play a crucial role in the formation of tungsten oxide nanorods.[10,16]

By adding hydrogen to the system, the back reactions are made favorable and tungsten oxide will be reduced rather than oxidized. Because of the volatility described above, the reaction conditions can greatly change the morphology of the final product. For example, when reducing WO_3 to W, changes in the reaction conditions can adjust

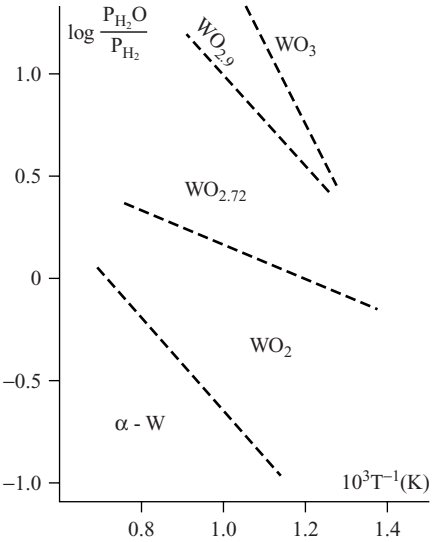

FIGURE 8.2. The stability of various tungsten oxides with respect to the ratio of the partial pressures of H_2O and H_2 and inverse temperature. Increasing this ratio and inverse temperature favor more oxidation.

the average grain size, the grain size distribution, grain shape, agglomeration, and more. With such versatility, it is no wonder this volatility of $WO_2(OH)_2$ is being harnessed to create one-dimensional morphologies. Nonetheless, much of the chemistry of tungsten oxide reduction is still described empirically today.[15] Some quantitative properties of this process will be presented in this chapter to the extent that they are known.

8.2.2. Thermodynamic and Kinetic Properties of WO_x Reactions

Based on the standard Gibbs free energy of the various oxides, three triple points can be calculated: $WO_{2.72}$, $WO_{2.9}$, WO_2 at about 600°C, $WO_{2.9}$, WO_3, WO_2 at about 270°C, and WO_2, $WO_{2.72}$, W at 1480°C. Using this data, a phase diagram can be constructed. The stability of the various oxides is shown in Fig. 8.2 with respect to the partial pressures of H_2O and H_2, and temperature. Because all of these compositions are equilibrium compositions, any of them can be produced simply by annealing W or WO_3 at the given partial pressure ratio and temperature.

As previously mentioned, the hydrated species $WO_2(OH)_2$ is the primary volatile species in the tungsten–oxygen–hydrogen system. This species can be formed from most forms of tungsten and its oxides. For example:

$$\begin{aligned}
WO_3(s) + H_2O(g) &\leftrightarrows WO_2(OH)_2(g)\\
\frac{1}{2}W_{20}O_{58}(s) + 11H_2O(g) &\leftrightarrows 10\ WO_2(OH)_2(g) + H_2(g)\\
W_{18}O_{49}(s) + 23H_2O(g) &\leftrightarrows 18\ WO_2(OH)_2(g) + 5H_2O(g)\\
WO_2(s) + 2H_2O(g) &\leftrightarrows WO_2(OH)_2(g) + H_2(g)\\
W(s) + 4H_2O(g) &\leftrightarrows WO_2(OH)_2(g) + 3H_2(g)
\end{aligned}$$

It is clear from these expressions that the partial pressure of water vapor should play a central role in determining the partial pressure of the volatile hydrate in the system, and indeed this is found to be the case. The partial pressure can be calculated from thermodynamic data and compared to that of other tungsten oxide species. Such calculations confirm that $WO_2(OH)_2$ is by far the most volatile tungsten-containing species in the tungsten–oxygen–hydrogen system. This volatility leads to chemical vapor transport of tungsten, which in turn can lead to the coarsening of grains in a powder or, under the proper conditions, the formation of nanorods.[15]

The final aspect of tungsten oxide reduction chemistry that needs to be considered is the kinetics of the reactions. Under most circumstances, the reduction of tungsten oxides is a transport limited process limited by the rate of transport of the water vapor product out of the material. Under such conditions, no "shortcuts" in the reduction path may be taken, with the WO_3 oxide being reduced according to the following path:

$$WO_3 \rightarrow WO_{2.9} \rightarrow WO_{2.72} \rightarrow WO_2 \rightarrow W$$

At high temperatures, these reactions occur discreetly, where one step essentially goes to completion before the next starts. This is not the case, however, below 750°C, where there can be overlap of reactions. Due to wide fluctuations in oxygen concentration throughout the reacting sample at these temperatures, some steps can be circumvented in oxygen-deficient regions. These two situations, high temperature and low temperature reduction, are compared in Fig. 8.3 and Fig. 8.4. These oxidation and reduction reactions, as well as their associated processes such as volatization, will play a key role in the discussion of the synthetic routes to $WO_{2.72}$ nanorods.

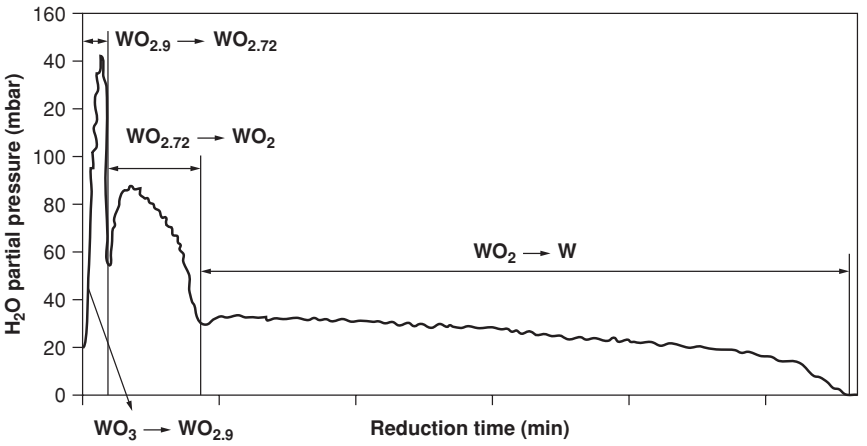

FIGURE 8.3. High temperature reduction of tungsten oxide. H_2O partial pressure is indicative of the rate of reduction. The four reduction steps are distinctly separated, indicating that the material passes through each equilibrium composition as it is reduced. From Lessner and Schubert.

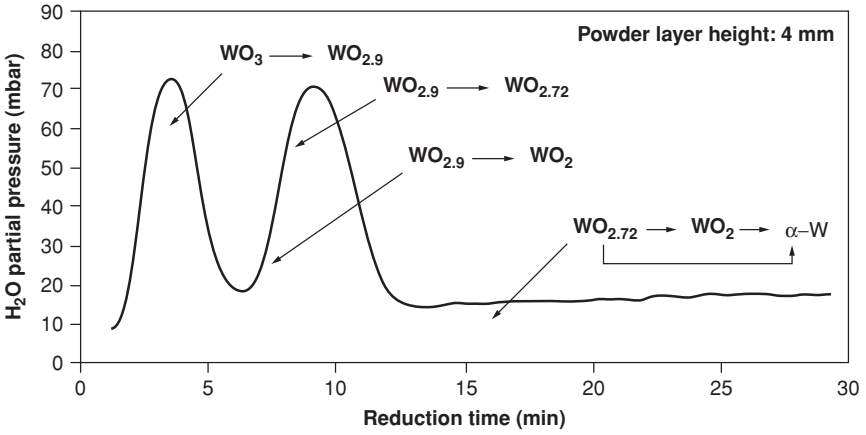

FIGURE 8.4. Low temperature reduction of tungsten oxide. Note that there are only two peaks, indicating that there must be some steps skipped in the $WO_3 \rightarrow W$ reduction. These skipped steps occur because of local variations in oxygen concentration. From Lessner and Schubert.

8.3. SYNTHETIC METHODS TO $WO_{2.72}$ NANORODS

Researchers have employed several strategies to achieve the one-dimensional growth that is necessary to create a nanorod. These strategies fall into several general areas. The simplest of these is relying on an anisotropic crystallographic structure of the desired solid to lead to anisotropic growth. Another route employed involves creating a liquid–solid interface on one face of the growing seed crystal. By reducing the symmetry of the seed so that reaction only takes place on that one face, this interface leads to one-dimensional growth, typically in a direction orthogonal to the interface. A wide variety of templates have also been employed to create one-dimensional nanostructures. These methods have included using solid substrates decorated with grooves or steps to "catch" sputtered, electrochemically plated, or electrodeposited material. Likewise, porous polymer or alumina membranes have been employed as templates for nanorod synthesis of metals, semiconductors, ceramics, and organic polymers. Such a wide variety of products suggest that this may be the most versatile method with respect to nanorod composition. In methods somewhat related to these porous membrane methods, nanorods have been templated against self-assembled rod-shaped micelles of surfactants. Finally, existing nanorods and other one-dimensional nanostructures have also been used to template nanorods. Using this approach, however, frequently results in polycrystalline nanorods, which are generally less desirable than the single crystalline nanorods generally prepared by the other synthetic methods.[9]

Vapor deposition techniques have been extensively studied for the fabrication of metal and metal oxide structures. Indeed, the first reported tungsten oxide nanorods were essentially grown by this method.[17] This groundbreaking synthesis of $WO_{2.72}$ leaves room for improvement, however, as it requires a reaction temperature of 1600°C in an argon atmosphere. Additionally, the researchers found the reaction product to be commingling $WO_{2.72}$ nanorods and WO_3 platelets rather than pure nanorods. Later,

other groups varied the reaction conditions, allowing tungsten oxide nanorods to be grown at lower temperatures (about 800°C).[10,18] Common among all three of these methods, as well as that developed by Liu *et al.*, is that tungsten is oxidized by an oxygen source such as SiO_2 or B_2O_3 that limits the availability of oxygen.[19] For example, the authors propose the following equations to describe the chemistry occurring in their experiments:

$$W + H_2O \rightarrow WO_x + H_2^{10}$$
$$W + SiO_2 \rightarrow WO_x + WSi^{17}$$
$$W + B_2O_3 \rightarrow WO_x + B_2O_2^{19}$$

In each case, an inert atmosphere is employed with the oxidizing agent being supplied in small concentrations. Presumably, the lack of available oxygen results in the substoichiomentric oxide. Indeed, Rothschild *et al.* noted that the aspect ratio of their nanorods declined as the vapor pressure of water in their reaction vessel increased.[20] Because the partial pressure of water directly affects the amount of oxidation, this may be an effect of further oxidation resulting in more isotropic crystal structures. Also, given the variety of oxidizing agents that have been used to produce tungsten oxide nanorods, it is likely that many other oxidizers could be employed as well, allowing the reaction conditions (and perhaps products) to be further optimized.

To allow a simpler, lower temperature route to tungsten oxide nanorods, some groups have turned to colloidal methods that have been used successfully to synthesize nanocrystalline metals and metal calcogenides.[21,22] These methods are generally considered to be cousins of vapor deposition and often called solution–liquid–solid methods.[9] Rather than using vaporized material as the source of tungsten for the oxide, these methods typically rely on dissolved organic tungstates such as $W(CO)_6$ or tungstic acid (H_2WO_4) as a tungsten source.[12,23,24] These methods afford lower reaction temperatures, which may allow better control over the nanorod product as well as lead to easier scale-up.[12,24]

In one such method, Park *et al.* mixed $W(CO)_6$, $Me_3NO{\cdot}2H_2O$, and oleylamine and allowed the slurry to react at about 270°C for about 24 h.[24] The solution eventually turned blue as tungsten oxide nanorods formed, which were precipitated out of the solution by adding ethanol. Unfortunately, the authors do not elaborate on this method and it is unclear what mechanism is at work here. The oleylamine added to the slurry acts as a surfactant, keeping the nanorods dispersed in suspension. While the relatively polar ethanol added to the relatively nonpolar solution presumably disrupts the interaction between the surfactant and the nanorods, allowing them to agglomerate and settle out.[25] No research, however, has investigated the role that the oleylamine surfactant plays in the formation of the nanorods in this particular reaction. It has been used as a surfactant for the size control of other nanoparticles however, suggesting that it is likely that oleylamine guides the formation of the nanorods in this case.[26]

It is worth reviewing how kinetic and thermodynamic factors generally affect the growth of nanostructures under the influence of surfactants. Though they used CdSe and PbS respectively to study the surfactant-assisted synthesis of nanorods, Peng *et al.* and Lee *et al.* have produced a pair of quite complimentary studies.[21,27] Peng *et al.* observed that kinetic control via monomer concentration was the principle factor in their growth

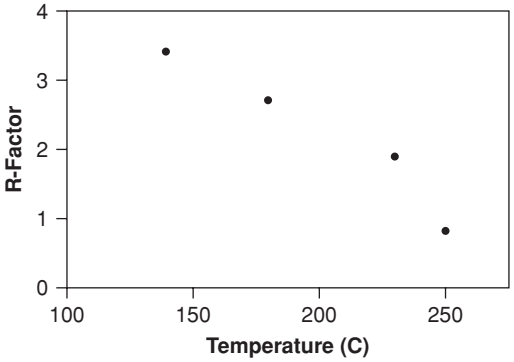

FIGURE 8.5. The effect of synthesis temperature on the anisotropy of PbS nanocrystals. Anisotropy is quantified by the R-factor (r_{100}/r_{111}, the ratio of the central distance of the $\{100\}$ faces to that of the $\{111\}$ faces). The decreasing trend is hypothesized to be due to the increased ability to overcome the activation energy necessary to grow the higher energy faces of the crystal at higher temperature. After Lee *et al*.

of CdSe nanorods. A high concentration of monomer, they found, drove the growth of the anisotropic c-axis at a much faster rate than the other axes (or possibly inhibited the growth of the a-and b-axes—they do not attempt to determine this), leading to high aspect ratio nanorods. Additionally, at high monomer concentrations, the smaller particles grew faster than the larger particles. Thus, by maintaining high monomer concentrations, Peng *et al.* were able to synthesize fairly *monodisperse*, high aspect ratio nanorods. It is clear that the surfactant is directing growth, but without better characterization of the surfactant's behavior in the system it cannot be determined whether rod-shaped surfactant micelles are formed or if the surfactant preferentially adsorbs to particular faces without first forming micelles.

Lee *et al.*[27] expand this research beyond the highly anisotropic crystals of CdSe to the more symmetric crystals of PbS. With such isotropic crystals, more tuning of the reaction conditions was necessary. First, they noted that higher aspect ratio materials result from lower reaction temperatures, as indicated in Fig. 8.5. As the reaction temperature is increased, they argue that the activation barrier to reaction on the less-favored faces is made negligible, and so the crystal grows isotropically. As even higher temperatures and longer reaction times are used, the reaction tends toward the thermodynamic equilibrium of isotropic crystals. Additionally, reducing the concentration of the surfactant led to decreased anisotropy, confirming that the surfactant does indeed block the growth of the crystal in two directions. Instead of the anisotropy of the unit cell contributing to anisotropy of adsorbed surfactant and hence growth, it is simply the difference in surface energy, in this case, between the $\{100\}$ (high energy) and $\{111\}$ (low energy) faces. Because of the complicated nature of these nanocrystals (not only rods but also star-like shapes), it is unlikely that growth is being guided by surfactant micelles.

Lou and Zeng spotted the work of Park *et al.* and sought to improve on it by developing an aqueous synthetic route.[12] In this method, water and sodium sulfate are added to freshly prepared tungstic acid and autoclaved at up to 200°C for up to 24 h (assuming saturated steam conditions, this corresponds to pressures of up to 15.5 bars).

By varying the amount of sodium sulfate and the reaction time, the size of these rods was controlled. Only centrifugation was necessary to collect the nanorods, indicating that rod–rod repulsion was minimal. Though the authors don't offer a detailed explanation for the mechanism of the reaction, they hypothesize that the sulfate ions may adsorb onto side surfaces or modify the ionic strength to allow the formation of nanorods. This will be discussed in the following section.

However, neither of these approaches addresses the issue of making large quantities of tungsten oxide nanorods at high purity that would allow for an efficient and facile scale-up. Walton *et al.* at the University of Sussex sought to address this issue with a novel synthetic method that involves passing water vapor over monocrystalline tungsten powder at 800°C.[10] Though this method requires high temperatures, Walton argues its superiority due to the simple mechanism, high product quality, and absence of harsh chemicals. Perhaps Walton is correct to point this out, but he ignores the work of Lou and Zeng, whose process involves just three inorganic chemicals and temperatures no higher than 200°C.[12] Without further research by scientists more knowledgeable about the scale-up process, a clear "winner" can hardly be declared.

Walton does offer a detailed explanation of a proposed growth mechanism. According to past research, WO_3 powders can be reduced with H_2 to form $WO_{2.72}$ nanorods. If allowed to react further, these continue to reduce to WO_2 agglomerates, as expected based on the general tungsten–oxygen chemistry framework. The presence of water vapor was shown to be the controlling factor in the process.[28] Additionally, another group demonstrated that water vapor is essential for the synthesis of tungsten oxide nanorods via tungsten filament oxidation.[20] Thus, Walton proposes the following two mechanisms—one direct and one indirect:

A. $W + xH_2O \rightarrow WO_x + xH_2$
B. (i) $W + 3H_2O \rightarrow WO_3 + 3H_2$
   (ii) $WO_3 + xH_2 \rightarrow WO_{3-x} + xH_2O$

Because Walton started with pure W and observed no WO_3 in the product, he concluded that his method likely follows the direct route. More likely, however, is a two-step oxidation–reduction process that generates volatile $WO_2(OH)_2$ as an intermediate, such as

(i) $W(s) + 2H_2O(g) \rightarrow WO_2(OH)_2(g) + H_2(g)$
(ii) $WO_2(OH)_2(g) + 0.28H_2(g) \rightarrow WO_{2.72}(s) + 1.28H_2O(g)$.

The reaction yielding $WO_2(OH)_2$ is necessary to provide a volatile species to form the nanorod morphology. Without it, mass transport would be exceedingly slow and the nanorod morphology impossible.

The colloidal synthetic routes, however, must follow a reaction path similar to B.(ii) because their reactant is not pure W but an oxidized form. Interestingly, however, neither Park nor Lou indicate that WO_3 is present in their product if produced under optimal conditions even though they note it as a major contaminant when some reaction conditions are used. While this might be expected based on the fact that they are reducing reactants such as WO_4^{2-}, where WO_3 could be an intermediate, it is possible that the reaction conditions do not permit the formation of that phase. This will be discussed further below.

8.4. CRYSTAL STRUCTURE AND GROWTH

Though the synthetic routes vary greatly among these three groups, they do all agree on the crystal structure and growth direction of the nanorods. All three identify their nanorods as $WO_{2.72}$, citing X-ray diffraction (XRD) data that confirms the crystals' monoclinic dimensions in agreement with the literature.[10,12,24] Furthermore, Park compares the intensities of the (010) and (014) peaks to bulk $WO_{2.72}$. Because the intensity of the peak resulting from (010) in the nanorods has increased by 2.25 times the (014) peak, he concludes that ⟨010⟩ must be the direction of growth. Walton's group cites similar data, while Zeng arrives at this conclusion citing the presence of two strong (0k0) rings in the electron diffraction pattern rather than X-ray diffraction data.

This growth direction, incidentally, corresponds to the close-packed plane of the monoclinic $WO_{2.72}$ crystal ($a = 1.828$ nm, $b = 0.3775$ nm, $c = 1.398$ nm, $\beta = 115.14^{\circ}$).[10,14] Tenne at the Weizmann Institute of Science and his collaborators have published a detailed study of the structure of this material.[29] Tenne describes the crystal as a collection of WO_6 octahedra—the same basic units as WO_3. However, these octahedra form a network of pentagonal columns interspersed with hexagonal channels (see Fig. 8.6). This complicated structure, they report, is not only highly anisotropic but also mechanically strong. For bulk ceramics, the usual mode is crack propagation—an applied stress is concentrated at a crack tip, which propagates through the material (in ductile metals, stresses typically cause defect motion before crack propagation can occur). Nanorods, however, are likely akin to optical fibers in their failure mode—that is, because of their dimensions (and also their growth mechanism) cracks must be formed at the atomic level. Thus, the material must fail by the breaking of chemical bonds, initially unaided by cracks. The energy necessary to "snap" a nanorod—that is, to break it across a plane normal to the growth axis—is the sum of all the chemical

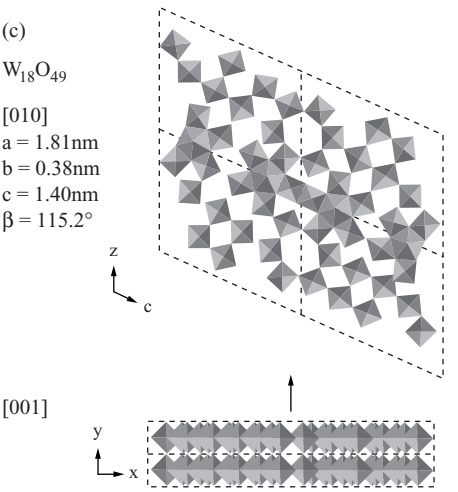

FIGURE 8.6. The crystal structure of $WO_{2.72}$ nanorods, showing the corner- and edge-sharing WO_6 octahedra that form pentagonal columns and hexagonal channels. From Frey *et al.*

bonds that cross that plane. Because of the complicated nature of the $WO_{2.72}$ crystal, many bonds must be broken to accomplish this and the stress in the crystal opposes crack propagation. The durable nature of these nanorods makes them especially suitable for applications such as scanning tunneling microscope (STM) tips and templates for nanotubes.[13]

Tenne is keen to note that the one-dimensional morphology is likely a *result* of the anisotropy of the $WO_{2.72}$ crystal, as has been shown for other materials.[9,29,30] This is ignored by the groups focusing on synthesis when they attempt to devise an explanation for their reactions. The morphology of the nanorods is dictated by the enhanced growth rate along the length of the nanorod. This enhanced growth rate, Tenne argues, is due to the differences in planar spacing of the crystal faces. Citing the Bravais–Friedel—Donnay–Harker (BFDH) law, he submits that the rate of growth should be inversely proportional to the planar spacing, which correctly predicts the morphology of the nanorods.[31] This is reasonable, as it will be energetically favorable to grow in the direction that causes the least increase in surface energy. Thus, the crystal will tend to grow faster in the direction of the shortest planar spacing because each additional plane causes a smaller increase in surface energy than adding a plane of larger spacing, making it more likely to occur. In $WO_{2.72}$, this ratio of planar spacings is about 5:1:1.3, which is in good agreement with the aspect ratio observed in the first reported tungsten oxide nanorods.[17]

Though Zeng recognized this growth direction, his explanation of the effect of the sulfate salt did not appear to be correct in light of the other synthetic methods.[12] He postulated that the salt might adsorb on the side surfaces of the growing nanorods, forcing them to grow into a rod-like morphology. It is more likely, however, that it is the crystal structure of the $WO_{2.72}$ nuclei that cause this morphology, as nanorods can be grown in situations without adsorbed molecules to confine growth (such as the vapor-phase growth described above). More likely is that the sulfate changes the ionic strength of the solution to a condition that favors the formation of the monoclinic $WO_{2.72}$ rather than WO_3 by lowering the activity of water. Figure 8.7 shows the effect of changing salt concentration on the formation of different phases. Because at high enough concentrations of sulfate WO_3 was totally absent in the product, it is probable that the sulfate moderates the rate of nucleation of the two species. By reducing the rate

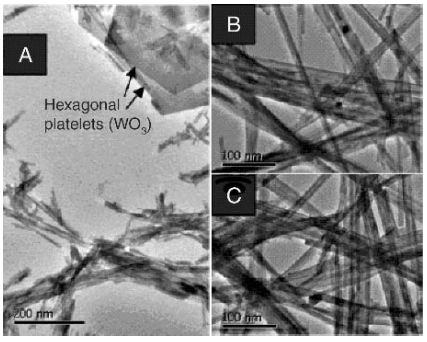

FIGURE 8.7. Effects of Na_2SO_4 content on $WO_{2.72}$ nanorod growth: (a) 2.5 g, (b) 5 g, (c) 10 g. WO_3 platelets contaminate a, but are absent in b and c. From Lou and Zeng.

of nucleation of WO_3 to zero, WO_3 crystals will not form. If sulfate instead controlled the rate of WO_3 growth, WO_3 would likely be present in the product but in the form of smaller crystals. Because this was not observed, sulfate is probably affecting the nucleation rate of WO_3. Perhaps an experiment could address this issue by using WO_3 seed crystals (if WO_3 appears in the product, sulfate controls nucleation) or examining the effects of reaction time on WO_3 formation at various sulfate concentrations (if WO_3 crystal size changes with sulfate concentration, sulfate affects WO_3 growth rate).

Similarly, Park was able to stimulate WO_3 platelet contamination by using elevated reaction temperatures. In this case, it seems clear that temperature is significantly increasing the activity of water, leading to more oxidation. The researchers also note that the temperature of the reaction can be used to control the length of the nanorods obtained, with higher temperatures resulting in longer nanorods with higher aspect ratios. This indicates that more is at work here than simply changing the activity of water. While this activity may control the phase that is formed, it probably doesn't control the aspect ratio. Instead, there must be some effect of temperature that makes the (010) face more reactive. Nonetheless, the resulting nanorods are a stable or metastable state, as longer reaction times do not lead to longer nanorods, indicating this effect is due to changing the thermodynamic equilibrium rather than enhancing the kinetics. This is a different behavior than Lee *et al.* observed when synthesizing the anisotropic PbS crystals described above.[27] In that study, which used surfactants to control the growth direction, they found that increasing temperature reduces the anisotropy. If nothing else, this seems to confirm that Park *et al.*'s $NaSO_4$ does not operate by the same mechanism as surfactants.

8.5. APPLICATIONS OF $WO_{2.72}$ AND OTHER TUNGSTEN OXIDES

8.5.1. Electro-Optical Properties and Quantum Confinement

A number of unique properties result from these characteristics. Some of the more exciting effects involve the nanorods' electrical and optical properties. Park's group noticed that little research had been done on the photoluminescence of nanostructured tungsten oxides.[24] They found that the strongest peaks occur at slightly different wavelengths for different nanorod lengths, with shorter nanorods emitting at shorter wavelengths. These photoluminescence spectra are shown in Fig. 8.8. The group concluded that this effect was the result of quantum confinement—that is, a band-to-band transition. Lou and Zeng also arrived at this same conclusion.[12] Essentially, this indicates that the dimensions of the material do not allow enough orbital–orbital interactions to form continuous valence and conduction bands. Hence, the electrons may only exist at discreet energy levels. The wavelength shift occurs as the electrons fall from the energy level that is the closest approximation to the bulk energy level normally excited by this wavelength.[32] Besides studying the physics of quantum confinement, this has important applications in the field of lasers and other electronics. Solid-state lasers are based on a 2-dimensional confinement (the electrons are free to move in 2 dimensions—a plane), which results in a highly functional but quite inefficient piece of equipment. By moving to lasers based on 1-dimensional confinement (allowing the electrons to move in only 1 dimension) made from, more efficient and powerful lasers may be possible.[32]

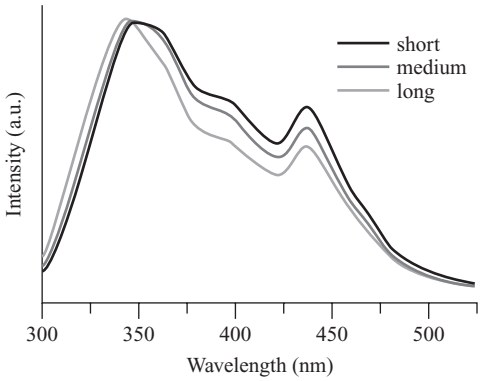

FIGURE 8.8. The photoluminescence spectra for short (25 nm), medium (75 nm), and long (130 nm) $WO_{2.72}$ nanorods. The main peaks are at ~345 nm and 437 nm. The 345 nm peak is likely a result of a band gap while the 437 nm peak is likely a result of oxygen defects. From Lee *et al*.

A higher energy peak was also investigated by Park's group. The wavelength of this peak, at 437 nm, was not dependent on the size of the nanorods used for the study, as shown in Fig. 8.8. Instead, the intensity of the peak was noticeably affected. Based on conclusions made by previous groups while studying the emission of WO_3 films, Park's groups suspects that this peak may originate from the presence of oxygen vacancies or defects.[3] Because longer nanorods were the result of faster growth (the reaction time for all nanorods was the same), it would be reasonable that these nanorods would have incorporated more defects, resulting in their higher intensity 437 nm peak. This justification would also explain why this peak is unaffected by nanorod dimension—presumably, this is because the band structures of the system are irrelevant to the emission.[24] Further study of this peak may lead to a method to analyze the quality of the nanorod crystal with respect to oxygen defects, which would be necessary to evaluate the appropriateness of different synthetic methods to applications such gas sensors, discussed below.

The oxygen defects that Park *et al.* use to explain the photoluminescent emission intensity at 437 nm also play a major role in the conductivity of tungsten oxides. Gillet *et al.* examined the electrical conductivity of annealed WO_3 films.[33] Though these films have a bulk stoichiometry different from $WO_{2.72}$ nanorods, as their surface stoichiometry changes they should fairly accurately model the electrical response of $WO_{2.72}$ nanorods. Indeed, depending on the processing conditions, the researchers found that surface oxygen vacancies could reach 50%, an oxygen concentration substantially less than that in $WO_{2.72}$. Gillet *et al.* found that the activation energy for surface conductivity in WO_3 films changed by a factor of more than two by changing the partial pressure of oxygen in the system from 0.2 mbar to 1 bar. This change in activation energy is manifested as a change in conductivity of about 3 orders of magnitude. The resistivity of these films is shown in Fig. 8.9 with respect to inverse temperature. The increase in oxygen vacancies lowers the activation energy of electrical conductivity—in this case, the ionization energy of the oxygen vacancies—because at higher concentrations the orbitals of the vacancies begin to overlap. This creates a "defect band," reducing the energy necessary to ionize these carriers. As the defect concentration increases, the band widens

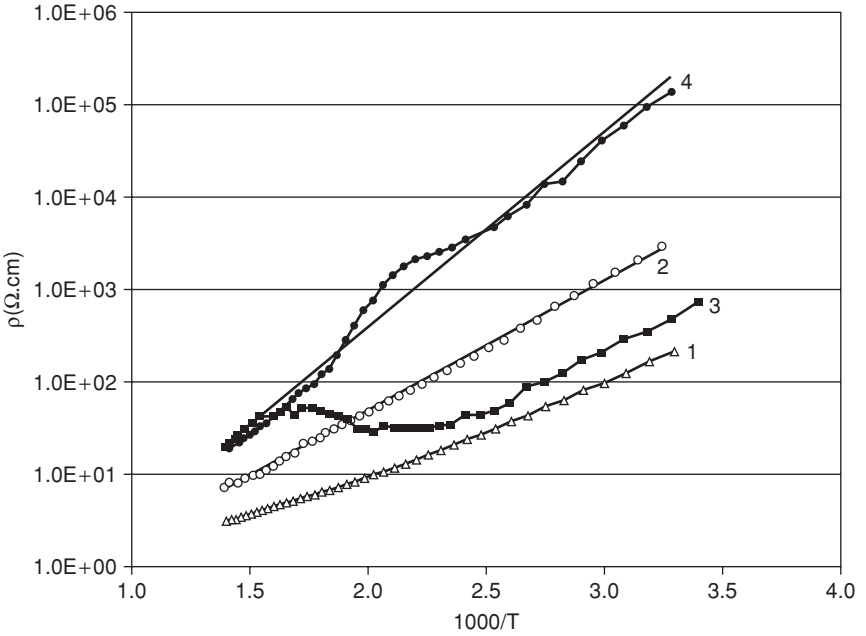

FIGURE 8.9. The resistivity of WO_3 films under various partial pressures of oxygen versus the inverse temperature. Curve 1 is in air, $P = 10$ mbar, curve 2 is in air, $P = 1$ bar, curves 3 and 4 are in oxygen, $P = 1$ bar. Curve 3 was recorded while increasing the temperature while curve 4 was recorded while decreasing the temperature. Note the strong dependence of resistivity on oxygen partial pressure. From Gillet *et al*.

to the point that it eliminates the band gap completely. $WO_{2.72}$ should lie somewhere in this defect range, and its electrical properties may be able to be probed further by testing WO_3 films (which are relatively easy to make) that have been processed so that their surface chemistry is identical to $WO_{2.72}$. Additionally, this study points out the importance of the environmental and processing conditions on tungsten oxides, and these cannot be ignored as studies are expanded to tungsten oxide nanorods.

The results of Gillet *et al.* and Park *et al.* suggest that some knowledge of the tungsten oxide band structure is necessary. Fortunately, in the course of their research on tungsten oxide–titanium oxide heterocatalysts, He *et al.* summarized the known electronic structure of WO_3.[4] The structure is represented graphically in Fig. 8.10, with the conduction-band-forming tungsten orbitals on the left side of the figure and the valence-band-forming oxygen orbitals on the right side. Because of the geometry of the WO_6 octahedra, the 5d orbital of the tungsten splits into a low energy t_{2g} level that points into empty space and a higher energy e_g level that points directly at the electronegative oxygen ion. Likewise, the 2p oxygen orbital splits into a high energy $2p_\pi$ that points into empty space and a lower energy $2p_\sigma$ orbital that points at the electropositive tungsten ion. The tungsten 5d and oxygen 2p orbitals are strongly hybridized. For perfect, defect-free WO_3, these energy levels result in a band gap of about 2.6 eV, but distortion of the crystal lattice by defects widens this gap.[34] However, by adding electrons to the structure, either by applying an electric field as in the case

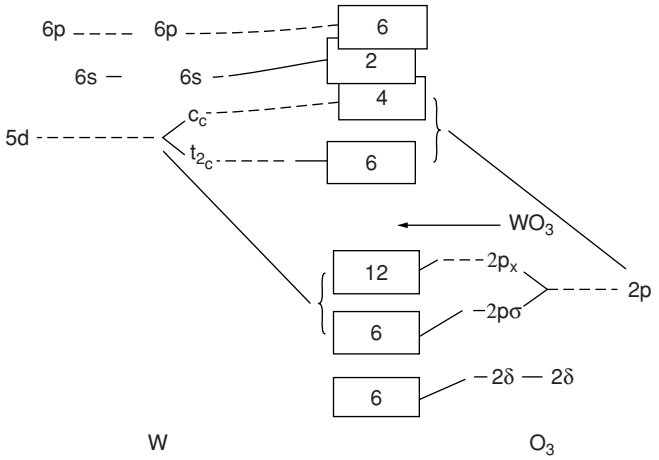

FIGURE 8.10. A representation of the band structure of WO_3. The W5d and O2p orbitals are strongly hybridized and correlated with each other, leading to the delocalization of the e_g and t_{2g} levels. From He *et al*.

with Gillet or by exposing the sample to sufficiently energetic photons, the valence and t_{2g} bands can be filled, resulting in W^{+5}.[4] The band gap of the W^{+5} state is smaller than that of WO_3. Thus, it may be the ease of creating these W^{+5} states that affects the band structure of $WO_{2.72}$ and causes it to appear blue. Because of the presence of W^{+5} in excited WO_3, WO_3 films can interact with visible light and also appear colored. Using this effect, tungsten oxides can be used as catalysts.

8.5.2. Use as Gas Sensors

Because the presence or absence of oxygen within the WO_x crystal lattice can have such a large effect on its conductivity, this material can have many uses as a sensor of oxygen-containing gases. It has even been shown to have the ability to sense H_2S, H_2, CS_2, and numerous hydrocarbons in addition to oxygen-containing compounds.[35] A good gas sensor has two main properties—its conductivity undergoes a large change in the presence of a particular gas due to high rates of adsorption, and the gas also desorbs quickly so that the sensor responds quickly to changing gas concentrations. Operating conditions play a large role in tuning the rates of adsorption and desorption. Sol–gel thin films offer a quick and easy method to make WO_3 thin films, and thus, gas sensors.[36] Galatsis *et al.* constructed WO_3 thin film sensors by this method and compared them to similar TiO_2 and MoO_3 sensors. Though they had inferior response to O_2, the WO_3 sensors excelled at detecting O_3, NO_2, and ethanol.[36] Choi *et al.* performed similar experiments, though they used hydrated tungsten oxide films.[37] They noted that their sensors could detect NO_2 concentrations at and below the environmental standard of 53 ppb.[38] This sensitivity, combined with the films' fast response time of about one minute suggests it as a very capable material for NO_2 sensing. By adjusting the calcination temperature and thus the pore sizes in the film, the group was able to optimize the film for high sensitivity (high calcination temperature) or fast response (low calcination

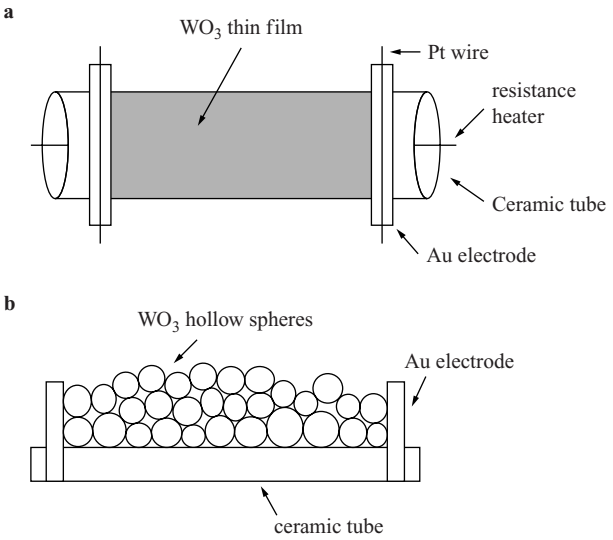

FIGURE 8.11. A schematic representation of the gas sensor designed by Li *et al.* An overview is given in a, while a cross-section is given in b. Tungsten oxide is coated onto an insulating ceramic cylinder and changes in conductivity of the coating are recorded. From Li *et al.*

temperature). A sensor that uses a series of various preparations of tungsten oxide films to quickly detect large concentrations of NO_2 and yet still be sensitive to trace amounts could be easily made.

Though they utilized a novel hollow-sphere form of WO_3 rather than $WO_{2.72}$ nanorods, the work of Li's group in researching tungsten oxide as gas sensors can be applied to the nanorod form.[35] Li's porous, hollow spheres were substituted for tungsten oxide polycrystalline films used in the previous studies by Galatsis *et al.* and Choi *et al.*[36,37] Thus, they overcome the sensitivity and selectivity problems caused by the surface structures and particle size of film approaches. As a result, only intermediate temperatures ($\sim$250°C) are required for operation. The spheres were dispersed in a solvent and subsequently applied to an insulating ceramic tube to form a film. Electrodes were connected to the film and a heater was added. A schematic is shown in Fig. 8.11. The sensors were found to be especially sensitive to hydrogen sulfide, ethanol, and acetone, with moderate sensitivity to other organics.

The sensing mechanism was related to changes in conductivity as molecules adsorbed onto the tungsten oxide. The sensitivity to adsorbed organics was hypothesized to be similar to that of the sensing properties of SnO_2 nanobelts. The cited study, by Yang *et al.* at Berkeley, provides good insight into this phenomenon.[39] Yang's tin oxide sensors rely on UV light to generate holes which cause the electron-trapping NO_2 to desorb, which increases the conductivity of the sensor. This prevents the sensor from becoming saturated with NO_2. Interestingly, Li's sensor uses elevated temperature rather than photogenerated holes to cause the adsorbed molecules to desorb. The effect is the same, but it would be interesting to confirm that the same effect can be obtained in tungsten oxide using photogenerated holes. Given that the band structure

can be "tuned" by changing the size of the nanorods and oxygen defects could change the sensitivity, this experimental device may lead to some interesting applications.[24] Additionally, the high aspect ratio of the nanorods affords a high surface to volume ratio, and the synthesis requires none of the complicated template synthesis necessary for Li's hollow spheres. The nanorods also offer an easily controllable platform for testing response to adsorbed molecules by testing the response of individual nanorods as opposed to polycrystalline films.

8.5.3. Tungsten Oxide Nanorods as Field Emitters

Field emitters lie at the heart of many familiar electronic devices. These include cathode ray tubes (such as those in televisions and computer monitors), X-ray generators, and microwave amplifiers.[40] These devices rely on the emission of electrons due to the presence of a large electric field. One-dimensional structures such as nanorods are ideal for such an application, as their "sharp" ends can generate very large electric fields that are difficult to attain in bulk materials, including fields upwards of 3 kV/μm.[41] As such, nanorods show promise for either high flux or low power applications. This potential was first recognized in carbon nanotubes, but investigations have since expanded to include zinc oxide, molybdenum oxide, and indium oxide materials. Armed with a technique to fabricate aligned arrays of $WO_{2.9}$ nanorods, Liu *et al.* sought to expand field emitter research to tungsten oxide materials as well (a method to produce aligned nanorods is essential so that the emitters are all aligned with respect to the applied electric field).[41] These researchers found that $WO_{2.9}$ nanorods had a remarkably low turn-on field (defined as the field necessary to obtain a current density of 10 μA/cm^2) of about 1.2 V/μm, which they report to be comparable to that of carbon nanotubes.

Li *et al.* performed similar experiments on quasialigned $WO_{2.72}$ nanorods, which also appear to be promising field emitters.[42] Using a similar experimental setup as Liu *et al.*, they found that the turn-on voltage was 2.6 V/μm, similar to that of $WO_{2.9}$. The group also investigated the threshold field—that is, the electric field necessary to generate a current density of 10 mA/cm^2. They report this value to be 6.2 V/μm, which is close to that of open-ended carbon nanotubes ($\sim$5 V/μm) and lower than that of SiC nanorods ($\sim$8.5 V/μm) and MoS_2 nanoflowers (7.6–8.6 V/μm). Thus, due to their low turn-on and threshold voltages, $WO_{2.72}$ nanorods appear to be excellent field emitters. However, while these two studies suggest that $WO_{2.9}$ nanorods are better field emitters than $WO_{2.72}$ nanorods because of their lower reported turn-on voltage, the data of Liu *et al.* and Li *et al.* should not be compared directly without some considerations. While this difference may be due to compositional differences, it may also be due to differences in nanorod alignment, measurement distance between the electrodes, and more.[41] Because neither group attempted to quantify these differences, comparisons between the two materials must be limited.

8.5.4. Tungsten Oxide as a Catalyst

Because of their electronic properties, particularly their visible-ultraviolet band gap, tungsten oxides have been the focus of a number of catalysis studies. Kohler and Gopel examined the electrocatalytic properties of $WO_{2.72}$ using spectroscopic surface

analytical techniques.[43] This method allowed them a detailed account of the chemical states present at the surface of $WO_{2.72}$ during aqueous reductions. They found that OH^- ions adsorb to the surface of the material and donate their electron to the surface cations. They observed this by using UPS to reveal that the surface tungsten ions were being reduced to a W5d1 electron state (the same state that was emphasized by Gillet *et al.* and Park *et al.*), which they argue is essential for the formation of adsorbed superoxide radicals.[24,33] Finally, their electromotive force experiments demonstrated that the activity of OH^- determines the activity of the adsorbed superoxide ions, where the tungsten surface acts to transfer an electron from the adsorbed OH^- to the adsorbing oxygen. It is the partially-reduced tungsten sites of the $WO_{2.72}$ electrode that facilitate these reactions.

Lindgren also investigated the electrocatalytic effects of tungsten oxide. In his work he used the more common WO_3 form to oxidize water, paying particular attention to the photoinduced nature of the process.[44] He found the material to be very promising, displaying such desirable characteristics as a low recombination rate of charge carriers and excellent kinetics. These properties resulted in good electron transfer over the WO_3 electrode and a quantum yield of nearly unity. Regardless, there are a number of difficulties that must be overcome. While thicker films tended to have better catalytic behavior, they were also more susceptible to cracking. Also, the band gap of defect-free WO_3 is about 2.6 eV, which is too large for the material to be efficient under solar radiation (silicon solar cells have a band gap of 1.1 eV, while only the largest band gap in a multi-band gap solar cell is 2.6 eV).[45]

Lindgren mentions that a possible solution to the problem of the large band gap is to construct a heterocatalyst of tungsten oxide and another metal oxide semiconductor. These sorts of heterocatalysts have been the focus of the studies of a number of groups. The catalyst is formed from tungsten oxide in conjunction with a common catalytic metal oxide such as those based on tin, zinc, or molybdenum. Of these three, tungsten oxide-zinc oxide catalysts seem to be the most studied, perhaps because of the higher melting point and lower cost of zinc.[46]

Because it also has a large band gap, combining zinc oxide with tungsten oxide will not solve the problem of solar powered oxidation. However, the large band gap does make for a large driving force for catalysis, allowing reactions with larger activation energies. In this case, Sakthivel *et al.* found that the photo-generated electrons created in the zinc oxide reduce sites in the tungsten oxide to a W^{+5} state.[47] This mechanism confirms that proposed by Kohler and Gopel, that reduced W^{+5} acts as the active catalytic site. As a result of this effect combined with enhanced charge carrier separation, Sakthivel *et al.* found that adding WO_3 to zinc oxide significantly enhanced its photocatalytic activity. Torres-Garcia *et al.* also investigated a WO_x–ZnO system for the purpose of oxidative desulfurization of oil refinery products.[48] They report that the stoichiometry of their tungsten oxide appears to be about WO_3 based on Raman spectroscopy. In comparative experiments to investigate the effect of tungsten concentration on the catalyst surface with catalyst activity, Torres-Garcia *et al.* found a direct relationship between high tungsten oxide concentrations and high catalytic activity. Equally important was their characterization of the surface structure and its effect on activity. They discovered that the highly faceted nature of many of the surfaces led to higher activity. This result suggests an important advantage of nanostructured materials over more conventional morphologies such as films: the surfaces

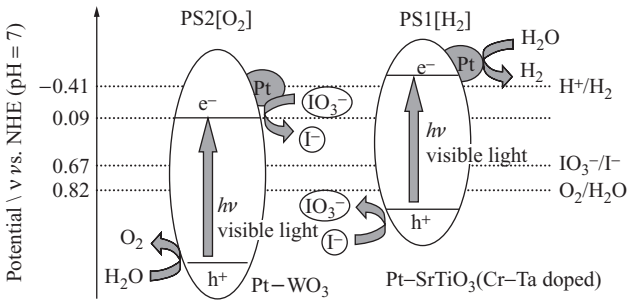

FIGURE 8.12. The speculated mechanism for the stoichiometric splitting of water with visible light using tungsten oxide and titanium oxide. Note the stair-step mechanism. From Sayama *et al*.

of these materials come to approximate these highly faceted surfaces. This effect can be demonstrated by drawing circles of various sizes on a display with discreet pixels. The stair-stepping effect in the display, analogous to faceting of materials, becomes more prevalent with respect to the image as the circle gets smaller. Use of nanorods as catalysts may allow the creation of highly reactive catalysts by taking advantage of this effect.

8.5.5. Tungsten Oxide and Titanium Oxide as a Heterocatalyst

Due to its near-ubiquity in fields ranging from catalysis to colloids to pigments, it is no surprise that titanium oxide has also been a frequent partner for tungsten oxides. In the realm of catalysis, as with pairing with zinc oxide, much of the interest in tungsten oxide–titanium oxide heterocatalysts is for photocatalytic applications. Sayama *et al.* used a system based on this pair of materials to stoichiometrically split water relying solely on visible light ($\lambda > 420$ nm) for the first time.[49] To accomplish this, they relied on the different potentials of the two materials' valence bands. Visible light excited electrons in the tungsten oxide materials. Using a IO_3^-/I^- redox mediator, this energy was shuttled to the titanium oxide material where light excited an electron to the conduction band, which in turn reduced H^+ to H_2. This stair-step mechanism is illustrated in Fig. 8.12. It is possible that the redox mediator could be eliminated if a suitable catalyst could be synthesized with the oxidation and reduction sites adjacent, resulting in a simplified energy diagram as shown in Fig. 8.13. Additionally, the highly active W^{+5} states of $WO_{2.72}$ could help increase the activity of this catalyst.

Lee *et al.* also investigated tungsten oxide–titanium oxide systems for catalysis, focusing on thin films.[50] The group found that this system improved on the photocatalytic properties of titanium oxide alone. The decomposition of methylene blue was used as a model reaction. Once again, the acidic surface of tungsten oxide is credited with the increase in reactivity. This confirms the previously mentioned finding that W^{+5} sites supply the bulk of the reactivity of tungsten oxide. Further evidence suggesting that it is the electronic structure of tungsten oxide that increases the reactivity of the system is the adsorption peak Lee *et al.* found at 410 nm. This peak corresponds well to the band gap of the tungsten oxide system and the effect of cutoff filters used in Sayama *et al.*'s work. Lee *et al.* also make note of the importance of charge carrier separation in the catalytic

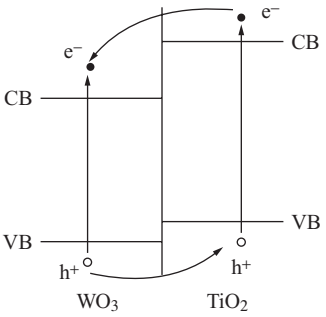

FIGURE 8.13. The energy diagram for the WO_3–TiO_2 system. Note how the energy difference between the lowest valence-band hole and highest conduction band electron is greater than the band gap of either material. From He *et al*.

process, discussing the effect of the traps for electrons and holes that the system generates and how these increase the efficiency of the reaction by preventing recombination.

8.5.6. Tungsten Oxide and Titanium Oxide as Colloids

Lee *et al.*'s study also investigates the hydrophilicity of the heterocatalyst. They mention that the highly acidic surface of the material is more hydrophobic than the pure titanium oxide surface. They theorize that this is because the acidic surface results in fewer adsorbed OH^- ions and thus a weaker interaction with water. As expected, this increased hydrophobicity leads to an increase in the stability of dispersions of nanoscale powders of this material.[51] Saltiel *et al.* showed that WO_3-coated titanium oxide powders were much more stable than their uncoated counterparts. Even after agglomeration, the agglomerates of the coated powders were more porous than those of pure titanium oxide (the coated powders had a fractal dimension of 1.55 while the pure titanium oxide powders had a fractal dimension of 1.60).

The effect of electron transfer between tungsten oxide and titanium oxide is also important in photochromatic applications. In an excellent study of aqueous sols, He *et al.* analyze the electronic structure of the tungsten oxide–titanium oxide system, finding that titanium oxide can catalyze the generation of W^{+5}.[4] This W^{+5} state is a colored state and can be generated from $WO_3 \cdot nH_2O$ by the following reactions:

$$WO_3{\cdot}nH_2O + h\nu \rightarrow WO_3{\cdot}(n - x/2)H_2O + xH^+ + xe^- + (x/4)O_2$$

$$WO_3{\cdot}(n - x/2)H_2O + x\,H^+ + xe^- + (x/4)O_2$$
$$\rightarrow {W^{6+}}_{(1-x)}{W^{5+}}_xO_{3-x/2}{\cdot}nH_2O + (x/4)O_2$$

In this case, titanium oxide is used both as a photocatalyst for the production of electrons and as a sink for holes, preventing recombination. This facilitates the reduction and thus the coloring of tungsten oxide. They also observe the effect of quantum confinement, resulting in band gaps in the sol that are greater than those normally observed in the bulk, as well as a blueshifted absorbance band, both results of the lack of orbital

overlap in the valence and conduction bands. These results have been confirmed by other studies.[34]

8.6. CONCLUSION

This chapter provides a detailed discussion on the synthesis, characterization, and applications of tungsten oxide nanorods. This sort of investigation of tungsten oxide, especially with a focus on the nanorod morphology, was previously unavailable. With this information collected, more informed decisions about the direction of tungsten oxide nanorod research can be made. In this course of reviewing the literature, it is clear that there is a relative dearth of characterization studies involving tungsten oxide nanorods (or, for that matter, and tungsten oxide other than WO_3). As a result, much of the discussions of tungsten oxide nanorods had to be inferred from WO_3 data. While this is certainly not ideal, it is immediately clear that WO_3 provides an excellent and well-understood basis for comparison. Thus, tungsten oxide nanorod researchers should be able to arrive at meaningful results and accurate interpretations of those results using the previously reported WO_3 experiments as a guide. The variety of synthetic pathways to tungsten oxide nanorods will hopefully open up synthesis to an equally wide variety of researchers. This will lead to more characterization studies and thus more application-based studies. As tungsten oxide nanorods show promise in a range of applications from gas sensing to catalysis, this will provide the science upon which those technologies can be developed.

REFERENCES

1. M. Stankova, X. Vilanova, E. Llobet, J. Calderer, C. Bittencourt, J. J. Pireaux, and X. Correig, Influence of the annealing and operating temperatures on the gas-sensing properties of rf sputtered WO_3 thin-film sensors, *Sensors Actuators* B **105**(2), 271–277 (2005).
2. S. Sekimoto, H. Nakagawa, S. Okazaki, K. Fukuda, S. Asakura, T Shigemori, and S. Takahashi, A fiber-optic evanescent-wave hydrogen gas sensor using palladium-supported tungsten oxide, *Sensors Actuators* B **66**(1–3), 142–145 (2000).
3. C. Paracchini and G. Schianchi, Luminescence of WO_3, *Physica Status Solidi A—Appl. Res.* **72**(2), K129–K132 (1982).
4. Y. He, Z. Wu, L. Fu, C. Li, Y. Miao, L. Cao, H. Fan, and B. Zou, Photochromism and size effect of WO_3 and WO_3-TiO_2 aqueous sol, *Chem. Mater.* **15,** 4039–4045 (2003).
5. M. A. Gondal, A. Hameed, and A. Suwaiyan, Photo-catalytic conversion of methane into methanol using visible laser, *Appl. Catal.* A **243**(1), 165–174 (2003).
6. C. Martín, G. Solana, V. Rives, G. Marcì, L. Palmisano, and A. Sclafani, Physico-chemical properties ofWO_3/TiO_2 systems employed for 4-nitrophenol photodegradation in aqueous medium, *Catal. Lett.* **49,** 235–243 (1997).
7. A. Shengelaya, S. Reich, Y. Tsabba, and K. A. Müller, Electron spin resonance and magnetic susceptibility suggest superconductivity in Na doped WO_3 samples, *Eur. Phys. J.* B **12**(1), 13–15 (1999).
8. L. Vayssieres, On the design of advanced metal oxide nanomaterials, *Int. J. Nanotechnol.* **1,** 1–41 (2004).
9. Y. Xia, P. Yang, Y. Sun, Y. Wu, B. Mayers, B. Gates, Y. Yin, F. Kim, and H. Yan, One dimensional nanostructures: Synthesis, characterization, and applications, *Adv. Mater.* **15**(5), 353–389 (2003).

10. Y. Z. Jin, Y. Q. Zhu, R. L. D. Whitby, N. Yao, R. Ma, P. C. P. Watts, H. W. Kroto, and D. R. M. Walton, Simple approaches to quality large-scale tungsten oxide nanoneedles, *J. Phys. Chem.* B **108**(40), 15572–15577 (2004).
11. I. Kaplan-Ashiri, S. R. Cohen, K. Gartsman, R. Rosentsveig, G. Seifert, and R. Tenne, Mechanical behavior of individual WS_2 nanotubes, *J. Mater. Res.* **19**(2), 454–459 (2003).
12. X. W. Lou and H. C. Zeng, An inorganic route for controlled synthesis of $W_{18}O_{49}$ nanorods and nanofibers in solution, *Inorganic Chem.* **42**(20), 6169–6171 (2003).
13. G. Gu, B. Zheng, W. Q. Han, S. Roth, and J. Liu, Tungsten oxide nanowires on tungsten substrates, *Nano Lett.* **2**(8), 849–851 (2002).
14. E. Lassner and W.-D. Schubert, *Tungsten - Properties, Chemistry, Technology of the Element, Alloys, and Chemical Compounds* (Kluwer Academic/Plenum Publishers, Norwich, NY, 2004) pp. 133–177.
15. E. Lassner and W.-D. Schubert, *Tungsten - Properties, Chemistry, Technology of the Element, Alloys, and Chemical Compounds* (Kluwer Academic/Plenum Publishers, Norwich, NY, 2004), pp. 85–109.
16. Y. Shingaya, T. Nakayama, and M. Aono, Epitaxial growth of WO_x nanorod array on W(001), *Sci. Technol. Adv. Mater.* **5**(4–5), 647–649 (2004).
17. Y. Q. Zhu, W. Hu, W. K. Hsu, M. Terrones, N. Grobert, J. P. Hare, H. W. Kroto, D. R. M. Walton, and H. Terrones, Tungsten oxide tree-like structures, *Chem. Phys. Lett.* **309**(5–6), 327 (1999).
18. D. Z. Guo, K. Yu-Zhang, A. Gloter, G. M. Zhang, and Z. Q. Xue, Synthesis and characterization of tungsten oxide nanorods, *J. Mater. Res.* **19**(12), 3665–3670 (2004).
19. Z. Liu, Y. Bando and C. Tang, Synthesis of tungsten oxide nanowires, *Chem. Phys. Lett.* **372**(1–2), 179 (2003).
20. A. Rothschild, J. Sloan, and R. Tenne, Growth of WS2 nanotubes phases, *J. Am. Chem. Soc.* **122**(21), 5169–5179 (2000).
21. X. Peng, L. Manna, W. Yang, J. Wickham, E. Scher, A. Kadavanich, and A. P. Alivisatos, Shape control of CdSe nanocrystals, *Nature* **404**(6773), 59–61 (2000).
22. N. R. Jana, L. Gearheart, and C. J. Murphy, Wet chemical synthesis of silver nanorods and nanowires of controllable aspect ratio, *Chem. Commun.* **7**, 617–618 (2001).
23. Y. Koltypin, S. I. Nikitenko, and A. Gedanken, The sonochemical preparation of tungsten oxide nanoparticles, *J. Mater. Chem.* **12,** 1107–1110 (2002).
24. K. Lee, W. S. Seo, and J. T. Park, Synthesis and optical properties of colloidal tungsten oxide nanorods, *J. Am. Chem. Soc.* **125,** 3408–3409 (2003).
25. T. S. Yoon, J. Oh, S. H. Park, V. Kim, B. G. Jung, S. H. Min, J. Park, T. Hyeon, and K. B. Kim, Single and multiple-step dip-coating of colloidal maghemite (g-Fe_2O_3) nanoparticles onto Si, Si_3N_4, and SiO_2 substrates, *Adv. Funct. Mater.* **14**(11), 1062–1068 (2004).
26. F. Dumestre, B. Chaudret, C. Amiens, M. Fromen, M. Casanove, P. Renaud, and P. Zurcher, Shape control of thermodynamically stable cobalt nanorods through organometallic chemistry, *Angew. Chem. Int. Ed.* **41**(22), 4286–4289 (2002).
27. S. M. Lee, Y. W. Jun, S. Cho, and J. Cheon, Single-crystalline star-shaped nanocrystals and their evolution: Programming the geometry of nano-building blocks, *J. Am. Chem. Soc.* **124**(38), 11244–11245 (2002).
28. V. K. Sarin, Morphological changes occurring during the reduction of WO_3, *J. Mater. Sci.* **10**(4), 593–598 (1975).
29. G. L. Frey, A. Rothschild, J. Sloan, R. Rosentsveig, R. Popovitz-Biro, and R. Tenne, Investigations of nonstoichiometric tungsten oxide nanoparticles, *J. Solid State Chem.* **162**(2), 300 (2001).
30. I. Kaplan-Ashiri, S. R. Cohen, K. Gartsman, R. Rosentsveig, G. Seifert, and R. Tenne, Mechanical behavior of individual WS_2 nanotubes, *J. Mater. Res.* **19**(2), 454–459 (2004).
31. J. Prywer, Correlation between growth of high-index faces, relative growth rates and crystallographic structure of crystal, *Eur. Phys. J.* B **25,** 61–68 (2002).
32. G. F. Strauss, *The Basics of Quantum Dots*. (2002) [Available from: http://www.chem.ucsb.edu/∼strouse_group/learning.html.
33. M. Gillet, C. Lemire, E. Gillet and K. Aguir, The role of surface oxygen vacancies upon WO_3 conductivity, *Surf. Sci.* **532–535,** 519–525 (2003).

34. T. He, Y. Ma, Y. Cao, X. Hu, H. Liu, G. Zhang, W. Yang, and J. Yao, Photochromism of WO_3 colloids combined with TiO_2 nanoparticles, *J. Phys. Chem.* B **106,** 12670–12676 (2002).
35. X. L. Li, T. J. Lou, X. M. Sun, and Y. D. Li, Highly sensitive WO_3 hollow-sphere gas sensors, *Inorganic Chem.* **43,** 5442–5449 (2004).
36. K. Galatsis, Y. X. Li, W. Wlodarski, E. Comini, G. Sberveglieri, C. Cantalini, S. Santucci, and M. Passacantando, Comparison of single and binary oxide MoO_3, TiO_2 and WO_3 sol-gel gas sensors, *Sensors Actuators* B **83**(1–3), 276–280 (2002).
37. Y. G. Choi, G. Sakai, K. Shimanoe, Y. Teraoka, N. Miura, and N. Yamazoe, Preparation of size and habit-controlled nano crystallites of tungsten oxide, *Sensors Actuators* B **93**(1–3), 486–494 (2003).
38. U.S. Environmental Protection Agency, *National Ambient Air Quality Standards*. (2005).
39. M. Law, H. Kind, B. Messer, F. Kim, and P. Yang, Photochemical sensing of NO_2 with SnO_2 nanoribbon nanosensors at room temperature, *Angew. Chem. Int. Ed.* **41**(13), 2405–2408 (2002).
40. P. Gröning, P. Ruffieux, L. Schlapbach, and O. Gröning, Carbon nanotubes for cold electron sources, *Adv. Eng. Mater.* **5**(8), 541–550 (2003).
41. J. Liu, Z. Zhang, Y. Zhao, X. Su, S. Liu, and E. Wang, Tuning the field-emission properties of tungsten oxide nanorods, *Small* **1**(3), 310–313 (2005).
42. Y. Li, Y. Bando, and D. Golberg, Quasi-aligned single-crystalline $W_{18}O_{49}$ nanotubes and nanowires, *Adv. Mater.* **15**(15), 1294–1296 (2003).
43. H. Kohler and W. Gopel, Catalysis of the oxygen reduction on $W_{18}O_{49}$ electrodes by OH^- induced surface-states—A study based on XPS UPS and electromotive-force measurements, *J. Electrochem. Soc.* **139**(11), 3035–3042 (1992).
44. T. Lindgren, *Photo Induced Oxidation of Water at Thin Film Electrodes: A study of Tungsten Oxide, Hematite, Indium Nitride and Tin Nitride, in Department of Physical Chemistry*. 2001, Uppsala University. p. 80.
45. K. M. Yu, W. Walukiewicz, J. Wu, W. Shan, J. W. Beeman, M. A. Scarpulla, O. D. Dubon, and P. Becla, Diluted II-VI oxide semiconductors with multiple band gaps, *Phys. Rev. Lett.* **91**(24), Art. no. 246403 (2003).
46. United States Geological Survey, *Minerals Information: Commodity Statistics and Information* (2004) [Available from: http://minerals.usgs.gov/minerals/pubs/commodity/.
47. S. Sakthivel, S. U. Geissen, D. W. Bahnemann, V. Murugesan, and A. Vogelpohl, Enhancement of photocatalytic activity by semiconductor heterojunctions:a-Fe_2O_3, WO_3 and CdS deposited on ZnO, *J. Photochem. Photobiol.* A **148,** 283–293 (2002).
48. E. Torres-García, G. Canizal, S. Velumani, L. F. Ramírez-Verduzco, F. Murrieta-Guevara, J. A. Ascencio, and E. Torres-Garcia, Influence of surface phenomena in oxidative desulfurization with WO_x/ZrO_2 catalysts,
Appl. Phys. A—Mater. Sci. Process. **79**(8), 2037–2040 (2004)
49. K. Sayama, K. Mukasa, R. Abe, Y. Abe, and H. Arakawa, Stoichiometric water splitting into H_2 and O_2 using a mixture of two different photocatalysts and an IO_3^-/I^- shuttle redox mediator under visible light irradiation, *Chem. Commun.* **23,** 2416–2417 (2001).
50. Y. C. Lee, Y. P. Hong, H. Y. Lee, H. Kim, Y. J. Jung, K. H. Ko, H. S. Jung, and K. S. Hong, Photocatalysis and hydrophilicity of doped TiO_2 thin films, *J. Colloid Interface Sci.* **267,** 127–131 (2003).
51. C. Saltiel, Q. Chen, S. Manickavasagam, L. S. Schadler, R. W. Siegel, and M. P. Menguc, Identification of the dispersion behavior of surface treated nanoscale powders, *J. Nanopart. Res.* **6,** 35–46 (2004).